Experimental investigations into the formation of nanoparticles in *a*/nc-Si:H thin films

S. Thompson
Department of Mechanical Engineering, University of Minnesota, Minneapolis, Minnesota 55455

C. R. Perrey and C. B. Carter
Department of Chemical Engineering and Materials Science, University of Minnesota, Minneapolis, Minnesota 55455

T. J. Belich and J. Kakalios
School of Physics and Astronomy, University of Minnesota, Minneapolis, Minnesota 55455

Uwe Kortshagen[a)]
Department of Mechanical Engineering, University of Minnesota, Minneapolis, Minnesota 55455

(Received 22 July 2004; accepted 18 November 2004; published online 18 January 2005)

Hydrogenated amorphous silicon thin films with nanocrystalline silicon inclusions (*a*/nc-Si:H) have received considerable attention due to reports of electronic properties comparable to hydrogenated amorphous silicon (*a*-Si:H) coupled with an improved resistance to the light-induced formation of defects. In this study, *a*/nc-Si:H thin films are synthesized via radio-frequency plasma-enhanced chemical-vapor deposition with helium and hydrogen diluted silane. The plasma conditions were chosen to simultaneously deposit both Si nanocrystallites and an amorphous silicon matrix. This structure has been confirmed by transmission electron microscopy (TEM) studies. Both plasma electronic diagnostics and TEM image analysis of *a*/nc-Si:H films deposited with and without a temperature gradient between the capacitively coupled reactor electrodes suggest nanoparticle formation in the plasma, as opposed to solid-state nucleation of the nanoparticles in the film. Optical-absorption studies of the *a*/nc-Si:H films indicate electrical properties comparable to *a*-Si:H. In particular, the evolution of the films' photoconductivity over light exposure time shows a Staebler–Wronski effect similar to *a*-Si:H. © *2005 American Institute of Physics*.
[DOI: 10.1063/1.1849435]

I. INTRODUCTION

Improved optical absorption in the visible portion of the spectrum together with reduced cost of production has made plasma-synthesized hydrogenated amorphous silicon (*a*-Si:H) the material of choice for photovoltaic applications.[1] However, extended illumination of *a*-Si:H-based solar cells results in the formation of metastable defects, a mechanism known as the Staebler–Wronski effect,[2] which greatly decreases the efficiency of the photovoltaic device. Recently, considerable attention has been given to materials synthesized by plasmas at the boundary of powder formation such as protocrystalline[3–7] and polymorphous silicon.[7–10] These nanostructured silicon films have been reported to have an enhanced stability against light-induced degradation.[3–10] Polymorphous silicon (pm-Si:H), reported by Roca i Cabarrocas and co-workers, is characterized by the presence of nanometer-sized crystalline silicon domains in an amorphous silicon matrix.[7,9–11] The deposition of pm-Si:H films, verified through spectroscopic ellipsometry studies, is reported to be critically dependent on the absence of a thermophoretic force that may prevent the deposition of silicon nanometer-sized crystals into the growing film.[8,12,13]

This paper reports experimental studies of hydrogenated amorphous silicon with nanocrystalline inclusions (*a*/nc-Si:H) with the aim of relating the deposition plasma characteristics to the films' structural and electronic properties. The *a*/nc-Si:H films have been deposited under conditions similar but not identical to those known to produce pm-Si:H films. A main distinction from studies aimed at polymorphous silicon deposition is the use of helium as an additional diluting gas. Films deposited using helium diluted silane have been reported to show improved transport properties, similar to results obtained for hydrogen dilution.[14] The plasma conditions are characterized through measurement of the electrical plasma parameters. Transmission electron microscopy (TEM) is used to characterize the structure and morphology of the *a*/nc-Si:H films. Nanocrystallite formation in the plasma, as opposed to solid-state nucleation of the nanocrystals in the film,[15] is suggested from plasma electronic diagnostics and TEM image analysis of *a*/nc-Si:H films deposited with and without a temperature gradient between the capacitively coupled reactor electrodes. The constant photocurrent method (CPM) is used to measure the key electronic properties of the *a*/nc-Si:H films. Photoconductivity measurements indicate that despite the nanocrystalline inclusions, *a*/nc-Si:H films show a Staebler–Wronski effect similar to *a*-Si:H films. A brief report of the preliminary results of this investigation has been previously published.[16]

This paper is organized as follows: Sec. II discusses the

[a)]Electronic mail: uk@me.umn.edu

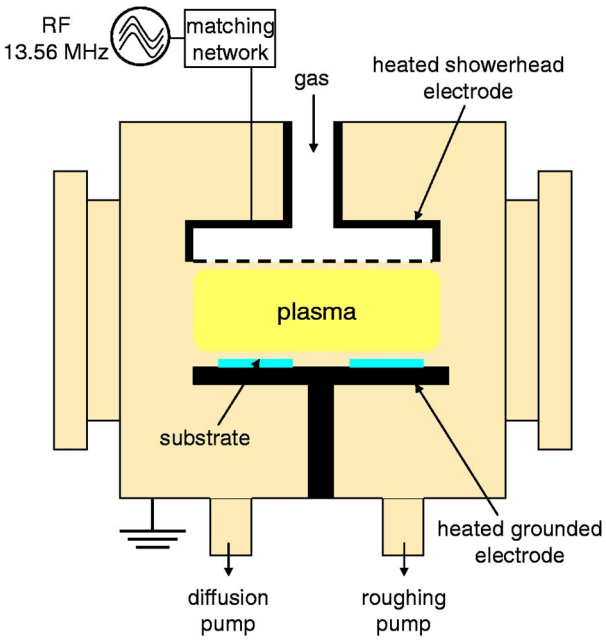

FIG. 1. Schematic of the rf-PECVD deposition system.

experimental methods. The results are presented and discussed in Sec. III. The main conclusions are summarized in Sec. IV.

II. EXPERIMENTAL METHODS

A. Sample preparation

The *a*/nc-Si:H films were deposited via rf plasma-enhanced chemical-vapor deposition (rf-PECVD) using a capacitively coupled plasma reactor operated at 13.56 MHz. Figure 1 shows a schematic of the plasma reactor. The upper showerhead electrode is rf powered; the lower grounded electrode supports the substrates. The interelectrode gap is 4 cm and both electrodes are approximately 16 cm in diameter. Both electrodes can be independently heated in a range from room temperature to about 300 °C to control the temperature gradient during the film deposition. The deposition conditions for the *a*/nc-Si:H and *a*-Si:H films are summarized in Table I. The *a*-Si:H films were deposited at a pressure of 100 mTorr with a rf power of 25 mW/cm^2 without hydrogen dilution. The *a*/nc-Si:H films were deposited at higher pressures, ranging from 1000 to 2000 mTorr, with an increased rf power of 100 mW/cm^2 utilizing hydrogen dilution. Additionally, both the rf electrode and the grounded electrode were heated to 250 °C during the *a*/nc-Si:H film deposition, whereas the grounded electrode was heated to 250 °C and the rf electrode was unheated for the *a*-Si:H films.

For the measurement of electrical and optical properties, films with thickness ranging from 150 to 500 nm were deposited on Corning 7059 glass substrates. Two coplanar chromium electrodes were evaporated onto the film surface and the contacts were verified to be ohmic. For structural studies by TEM and high-resolution TEM (HRTEM), films with an approximate thickness of 10 nm were deposited on cleaved NaCl substrates.[17] The films were then floated off in distilled water and collected on 3-mm Cu TEM grids; the specimens were then allowed to dry for 24 h in a dessicator before TEM examination.

B. Plasma characterization

The detection of particle nucleation and growth in the plasma is useful in applications where particles of a controlled size are desirable. Despite previous studies, the connection between the particle growth and the plasma discharge parameters is not fully understood.[18] In addition, the detection of particles with a size <10 nm in the plasma, by methods such as laser light scattering, has proven to be difficult.[19–22] Examination of the discharge electrical properties is a noninvasive diagnostic that provides information regarding the presence of particles in the discharge. Several studies have determined that the discharge impedance is strongly affected by particle nucleation,[18,20,22–27] becoming more resistive when particles are present.[22–24] With the onset of particle nucleation, significant variations in higher-order harmonics have been reported[21,25,26] as well as a sensitivity of the phase angle or shift between the discharge current and voltage wave forms.[18,24,27]

The current and voltage characteristics of the discharge were examined simultaneously using a Picoscope 212-100 oscilloscope. The current signal was obtained using a Pearson 2877 wideband current monitor and the dividing capacitor voltage probe (1/100) was used to monitor the voltage. The diagnostic probe is located at the rf feedthrough to the chamber, after the rf signal has passed through the matching network. The rf voltage is observed to be close to sinusoidal, as described by the relation

$$V(t) = V_{rf}\cos(\omega t). \tag{1}$$

The phase angle φ between the current and voltage was deduced from the measured time lag Δt between the peaks of the signals using the following relation:

TABLE I. Deposition conditions for the *a*-Si:H and a/nc-Si:H films.

Pressure (mTorr)	Flow-rate SiH_4/He (5:95) (sccm)[a]	Flow-rate H_2 (sccm)	Power (W)	T_{rf}/T_{subst} (°C)[b]	Material
100	19	0	5	—/250	*a*-Si:H
1450	40	100	20	250/250	*a*/nc-Si:H
1800	40	100	20	250/250	*a*/nc-Si:H

[a]Denotes Standard cubic centimeter per minute.
[b]Unspecified temperature (—) indicates that the electrode was not heated.

TABLE II. Plasma conditions used in examining the rf signal characteristics.

Pressure (mTorr)	Flow-rate SiH_4/He (5:95) (sccm)[a]	Flow-rate H_2 (sccm)	Power (W)	T_{rf}/T_{subst} (°C)[b]
100	19	0	5	—/250
250	30	0	5	—/250
600	40	100	20	250/250
1100	40	100	20	250/250
1500	40	100	20	250/250
1800	40	100	20	250/250

[a]In the case of the pristine He and H_2 plasma, the conditions used were identical to the above, with the exception that the SiH_4/He flow is replaced by pure He.
[b]Unspecified temperature (—) indicates that the electrode was not heated.

$$\phi = 2\pi\left(\frac{\Delta t}{T}\right), \tag{2}$$

where T is the period of the signals. To correct for offset in the angle, the phase angle between the current and voltage signals was measured under vacuum without plasma, and the plasma phase angle values were adjusted accordingly. Additionally, the effective power dissipated in the discharge P_{eff} was calculated from the amplitude of the measured current I_0, voltage amplitude V_0, and φ,

$$P_{eff} = \frac{1}{2} I_0 V_0 \cos(\varphi). \tag{3}$$

Changes in the phase angle and the dissipated power were measured under various silane (SiH_4) dilution and pressure conditions to monitor the effect of particle formation on the plasma. Subsequently these conditions were then compared to the pristine plasma conditions without silane. The experimental plasma conditions utilized in this study are presented in Table II. The silane plasma conditions utilized in this study were selected to be identical to those used to produce the films. Low pressures (100–250 mTorr), SiH_4 diluted only with He, and a rf power of 5 W were used to reproduce the *a*-Si:H plasma conditions. For the *a*/nc-Si:H plasma conditions, higher pressures (>500 mTorr), SiH_4 diluted with He and H_2, and 20 W of rf power were used. These conditions were repeated for the pristine plasma where He and He/H_2 were used instead of SiH_4/He and SiH_4/He/H_2, respectively.

C. Materials characterization

Preliminary TEM studies utilized a Philips CM30 operating at 300 kV. HRTEM imaging was performed in the aberration-corrected Philips CM200 at the Forschungszentrum Jülich, Germany. This instrument is equipped with a field-emission gun and a computer-controlled system for the correction of spherical aberration of the objective lens.[28–34]

The optical-absorption properties of the film samples were examined using the CPM.[35,36] CPM measurements of the spectral dependence of the optical-absorption coefficient were performed at room temperature after dark annealing the samples at 170 °C for 1 h. From these measurements the Urbach energy, Tauc optical gap, and approximate defect density are obtained.[35–42] Additional electronic properties and light-soaked behavior of the films were examined through measurements of the photo- and dark conductivities.[1] These measurements were performed under vacuum at 47 °C using ~100 mW/cm^2 heat-filtered white light illumination from a W–Ha lamp. The Staebler–Wronski effect was examined through measurements of the photoconductivity σ_{ph} as a function of light exposure time.

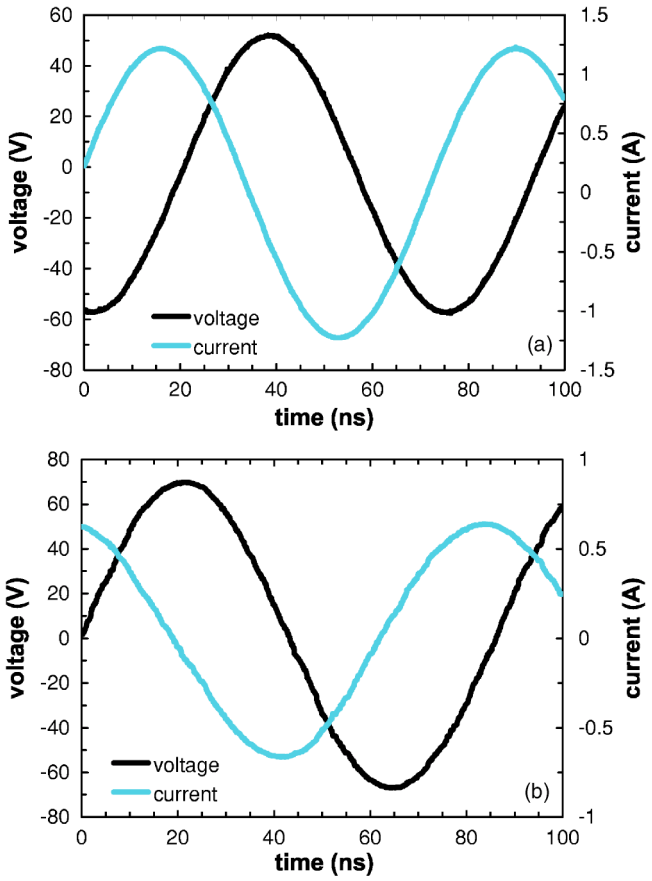

FIG. 2. Typical current and voltage characteristics obtained for the 1500-mTorr silane plasma conditions (A) and 1500-mTorr pristine plasma conditions (B).

III. RESULTS AND DISCUSSION

Changes of the discharge electrical properties were measured as indicators of particle nucleation and growth in the plasma. Figure 2 shows typical current and voltage signals for the 1500-mTorr *a*/nc-Si:H silane plasma conditions (A) and the pristine plasma conditions (B). For both conditions, the current and voltage display a sinusoidal wave form. The current is observed to be slightly anharmonic at lower pressures, for both the silane and pristine plasmas, which is consistent with other reports.[24]

The phase angle between the rf current and voltage was found to be most sensitive to changes in the plasma conditions. The phase angles for the silane and pristine plasma conditions are presented as a function of discharge pressure in Fig. 3. For the pristine plasma the magnitude of the phase angle is nearly constant at a value of 84° over the range of pressures examined. Under the conditions used to produce

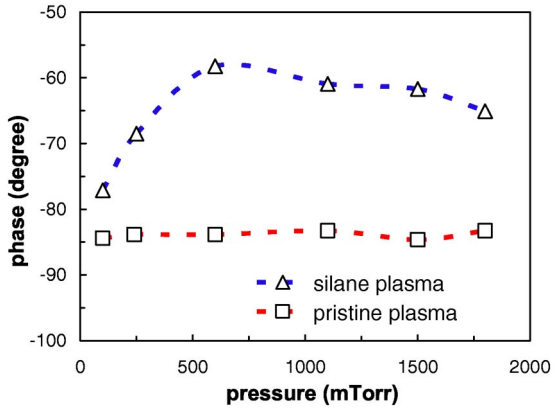

FIG. 3. Effect of SiH_4 to the phase angle between the rf current and voltage, with offset correction, presented as a function of discharge pressure for the pristine and silane plasma conditions.

a-Si:H (100–250 mTorr, without hydrogen dilution) particle formation in the plasma is not expected, since the silane partial pressure is only between 5 and 12.5 mTorr. In this region, the phase angle of the silane plasma is close to that of the pristine plasma. As the pressure is increased (>500 mTorr) and hydrogen dilution is added, the silane plasma transitions into the regime in which *a*/nc-Si:H film deposition is expected. In this plasma regime a significant shift in the phase angle from the pristine plasma condition occurs, reflecting an increase in the plasma resistance, most likely due to the formation of particles in the plasma, consistent with other reports.[21–25]

The effective power dissipated in the plasma P_{eff} was examined relative to the power measured at the rf generator output P_{input}. Figure 4 shows the ratio $P_{\text{eff}}/P_{\text{input}}$ for the pristine and silane plasmas over the range of pressures explored. In the case of the pristine plasma, no significant variation is observed with the increase of the discharge pressure. The effective power for the silane plasma is less than 10% of the input power. This is supported by the reported findings of pristine plasma studies, the power delivered to the discharge is significantly less than the power measured at the output of

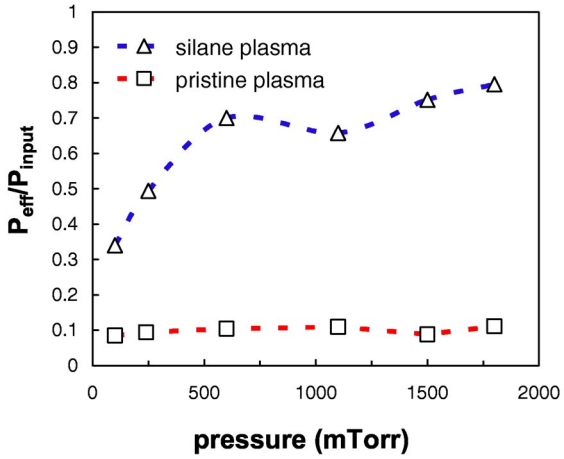

FIG. 4. Effective power dissipated in the plasma discharge P_{eff} relative to the power measured at the output of the rf generator P_{input} plotted for the silane and pristine plasmas as a function of discharge pressure.

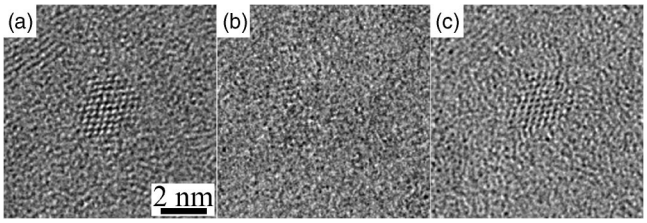

FIG. 5. High-resolution TEM through-focus image series of a Si nanoparticle. The contrast of the nanocrystal changes systematically as the focus is changed, while the contrast from the amorphous film does not change systematically in these three images.

the rf power generator.[20,24,43] However, in the case of the silane plasma, the effective power increases to nearly 80% of the input power at higher pressures. This observation is consistent with the measured shift in the phase angle as the plasma conditions transition from the *a*-Si:H regime to the *a*/nc-Si:H regime. These measurements of the plasma's electrical properties suggest that particle formation occurs at higher pressures (>500 mTorr) but is insignificant at lower pressures (<250 mTorr).

In order to correlate the film properties with the observed changes in the electric discharge properties, TEM and HRTEM studies of the deposited films were performed. In the *a*/nc-Si:H regime at pressures >1000 mTorr, nanocrystals embedded in an amorphous silicon matrix were observed. A series of HRTEM images of a representative Si nanocrystal taken at different defocus values is shown in Fig. 5. This focal series shows that as the focus is changed from overfocus [Fig. 5(a)] to underfocus [Fig. 5(c)] the contrast of the lattice fringes changes systematically. Such a contrast change is characteristic of crystalline materials when imaged in HRTEM.[17,44] This systematic behavior is not observed for the amorphous material surrounding the nanocrystal; instead, the contrast for the amorphous matrix changes little as the defocus is varied. Careful analysis of such images has shown that the Si nanocrystals are diamond cubic in structure with a lattice constant consistent with bulk Si.[45,46] Additionally, some nanoparticles contained twin boundaries and stacking faults characteristic of Si.[45,46] No alternative structures of Si have been observed in these films, as have been reported in other studies.[47–49]

To further elucidate whether the nanocrystals observed in the *a*/nc-Si:H films are indeed formed by nucleation in the gas phase and subsequently deposited into the film, experiments were performed using the thermophoretic force to either allow or prevent particle deposition on the substrate. The effect of thermophoresis on the structure of the films deposited in the *a*/nc-Si:H regime was examined through a TEM study of films deposited at 1450 mTorr. If the nanoparticles nucleate in the plasma and deposit in the film matrix, then a temperature gradient "pushing" the particles away from the film should inhibit their inclusion into the film and yield an amorphous material. To ascertain the amount of crystalline material in the films, dark-field TEM imaging was used. Regions that satisfy the Bragg diffraction condition at the position of the objective aperture will appear bright in these dark-field images.[17] Figure 6 shows dark-field (DF) TEM images from typical regions of the film deposited at

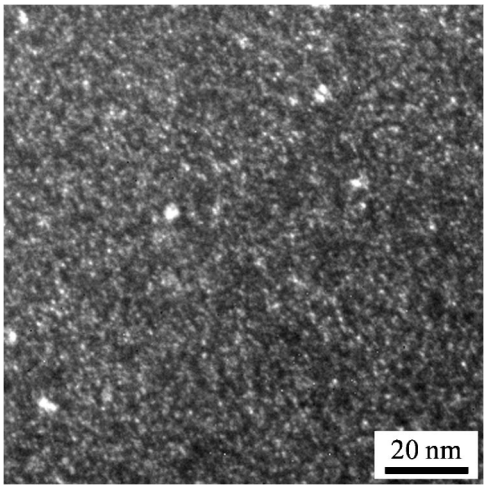

FIG. 6. Dark-field TEM image of a film deposited under the 1450-mTorr standard *a*/nc-Si:H conditions (both electrodes heated to 250 °C) that contains Si nanocrystals. In this image, the crystals that are diffracting at the position of the objective aperture in the TEM will appear bright; some nanoparticles approximately 5 nm in size are visible.

1450 mTorr without a temperature gradient, that is with both electrodes heated to 250 °C, as is the standard condition for the *a*/nc-Si:H film deposition. This film shows the characteristic *a*/nc-Si:H structure; crystalline regions of approximately 5 nm that are appropriately oriented can be identified within the amorphous matrix. The DF image of the film deposited in the presence of a temperature gradient, using an unheated rf electrode and 250 °C grounded electrode, under the 1450-mTorr *a*/nc-Si:H plasma conditions is shown in Fig. 7. This film does not appear to contain crystalline material and is amorphous. Thus in the presence of a temperature gradient pushing plasma-formed particles away from the growing film, *a*/nc-Si:H films are not observed. The observed effect of thermophoresis on the resulting film structure is consistent with the findings reported for pm-Si:H.[8,12,13]

Measurements of the bulk films' optical-absorption spectra were obtained from the CPM measurements. To compare the relative magnitude of the defect densities, which are proportional to the absorption coefficient at 1.2 eV, the samples were also examined using photothermal deflection spectroscopy (PDS). The experimental details of this measurement are available elsewhere.[50] The resulting absorption coefficient at 1.2 eV, the CPM derived Urbach energies, and the Tauc optical gaps are presented in Table III.

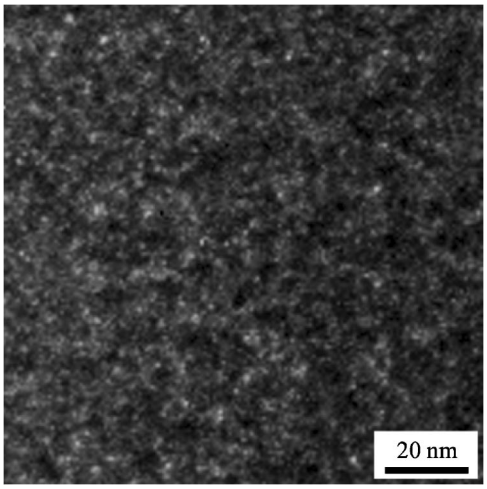

FIG. 7. Dark-field TEM image of a film deposited with the 1450-mTorr *a*/nc-Si:H conditions in the presence of a temperature gradient (unheated rf electrode) which appears to be amorphous. No nanocrystals of Si are identifiable in this image.

TABLE III. Optical-absorption coefficient evaluated at 1.2 eV, Urbach energy, and Tauc optical gap of the *a*/nc-Si:H and a-Si:H films.

Pressure (mTorr)	Material	α (1.2 eV) cm^{-1}	E_0 (meV)	E_g Tauc (eV)
100	*a*-Si:H	4[a]	43	1.69
1450	*a*/nc-Si:H	3	54	1.77
1800	*a*/nc-Si:H	2.5	51	1.74

[a]The α(1.2 eV) value the 100-mTorr *a*-Si:H film was estimated from the PDS measurements.

The *a*-Si:H film, deposited at 100 mTorr, exhibits an Urbach energy and Tauc optical gap values that are typical for standard amorphous silicon. The *a*/nc-Si:H films, deposited at 1450 and 1800 mTorr, show slightly broader Urbach energies and wider optical gaps compared to the *a*-Si:H film. Nonetheless, the *a*/nc-Si:H films' Urbach energies and optical gap values are consistent with those of high-quality *a*-Si:H films.[51] The optical-absorption coefficient at 1.2 eV photon energy, representing the midgap defect density of states, ranges from 2.5 to 4 cm^{-1} for the different film conditions, corresponding to midgap dangling-bond defect densities of $(3-4)\times 10^{16}$ cm^{-3}.[52] No significant decrease or increase in the defect density is observed for the *a*/nc-Si:H films despite the inclusions of nanocrystals in the film matrix. This is a marked difference with respect to pm-Si:H, for which a lower midgap defect density than *a*-Si:H films has been reported.[7,9]

The kinetics of the degradation of the films' photoconductivity on light exposure was examined in order to determine the films' stability with respect to light-induced defect creation (the Staebler–Wronski effect). Figure 8 shows the decay of the photoconductivity with the light exposure time. The initial photoconductivities, at an exposure time of 1 s, for the *a*/nc-Si:H and *a*-Si:H films are nearly identical. A light-induced degradation of almost one order of magnitude

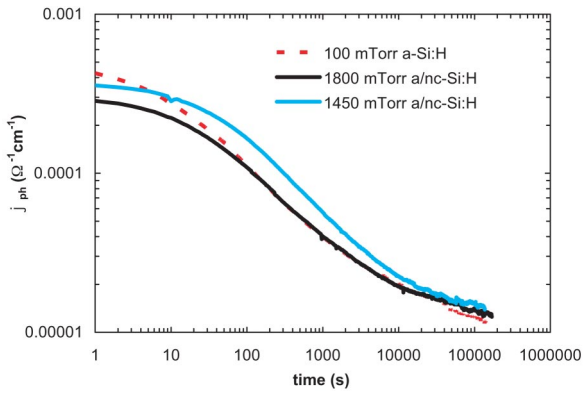

FIG. 8. Photoconductivity measured as a function of light-exposure time for the 100-, 1450-, and 1800-mTorr films.

is observed for both the *a*/nc-Si:H and *a*-Si:H films, with no appreciable difference in the rate or magnitudes of degradation. No improved resistance to the Staebler–Wronski effect is observed for the *a*/nc-Si:H film, contrary to the findings reported for the pm-Si:H films.[7,9,10]

Most of the parameters used in the present study are very similar to reports in which pm-Si:H films were produced.[7,9,10] These include the total gas flow rate, the silane flow rate (about 30% lower in this study), and the plasma chamber dimensions. However, it appears that there are two main differences between the deposition conditions used here compared to those reports. First, the present studies used a dilution of silane in a mixture of helium and hydrogen. pm-Si:H films were reported for either a dilution in helium[53] or hydrogen.[7,9,10] Since improved film properties were reported for both helium[53] and hydrogen[7,9,10] dilution, it is unlikely that a mixture of both gases should have a negative effect. The second difference, which may be more important for the difference in film properties in this study and in pm-Si:H studies, may be in the design of the discharge chamber. Polymorphous silicon films were obtained in discharge chambers in which the plasma is bounded by a confining plasma box.[9] The present deposition reactor does not use such a plasma confining box. It is thus possible that the presence of the heated electrodes and the cold reactor walls leads to a loss of clusters and small silicon nanocrystals to the reactor walls, causing a lower concentration of these species in the films. The presence of clusters and nanocrystals, however, is usually credited with the improved properties of pm-Si:H films.[13] In a recent study,[26] the authors had pointed out that even the presence of two small slits acting as optical windows in the plasma confining box can lead to a significantly different concentration of clusters and nanocrystals in the plasma.

IV. CONCLUSIONS

Hydrogenated amorphous silicon thin films were deposited by rf-PECVD under conditions of helium dilution with and without hydrogen dilution. Increased gas pressure and strong hydrogen dilution yielded *a*/nc-Si:H films with Si nanocrystallites embedded in an amorphous Si matrix, as confirmed by the TEM and HRTEM studies. The studies of the electrical discharge properties are consistent with the particle formation within the plasma in the *a*/nc-Si:H film regime. The studies using the thermophoretic force to either allow or prevent particle deposition into the films provide further evidence that the nanocrystallites observed in the *a*/nc-Si:H films are indeed formed in the gas phase and then included into the growing films, rather than formed by solid-state nucleation within the film matrix.

Through the examination of the optical-absorption coefficient, the *a*/nc-Si:H films were found to have electronic properties similar to those of the *a*-Si:H films. Additionally, no significant difference in the deep defect density of the films was observed. The *a*/nc-Si:H and *a*-Si:H films showed nearly identical photoconductivities and comparable magnitudes of decrease in the photoconductivity and dark conductivity with extended light exposure. In contrast to the studies on pm-Si,[7–10] no appreciable enhanced resistance to the Staebler–Wronski effect for the *a*/nc-Si:H films, related to the inclusion of nanocrystallites into the seemingly amorphous matrix, was observed in this study.

ACKNOWLEDGMENTS

This work is supported by NSF under IGERT Grant No. DGE-0114372 and DOE Grant No. DE-FG02-00ER54583. Two of the authors (C.R.P. and C.B.C.) acknowledge support from the 3M Heltzer Endowed Chair and the University of Minnesota Doctoral Dissertation Fellowship. Two other authors (T.J.B. and J.K.) are supported by NREL/AAD-9-18668-13. Four of the authors (S.T., T.J.B., J.K., and U.K.) acknowledge partial support by the NSF MRSEC DMR-0212302. The assistance of John Vinar and Dr. P. C. Taylor at the University of Utah for measurements of the PDS absorption spectra is gratefully acknowledged. Dr. Markus Lentzen and Professor Knut Urban, Research Center Jülich, provided access and assistance with the aberration-corrected HRTEM.

[1] R. A. Street, *Hydrogenated Amorphous Silicon* (Cambridge University Press, Cambridge, 1991).
[2] D. L. Staebler and C. R. Wronski, Appl. Phys. Lett. **31**, 292 (1977).
[3] Y. Lubianiker, J. D. Cohen, H.-C. Jin, and J. R. Abelson, Phys. Rev. B **60**, 4434 (1999).
[4] C. R. Wronski, J. M. Pearce, R. J. Koval, X. Niu, A. S. Ferlauto, J. Koh, and R. W. Collins, Mater. Res. Soc. Symp. Proc. **715**, 459 (2002).
[5] D. Kwon, C.-C. Chen, D. J. Cohen, H.-C. Jin, E. Hollar, I. Robertson, and J. R. Abelson, Phys. Rev. B **60**, 4442 (1999).
[6] R. Koval *et al.*, Mater. Res. Soc. Symp. Proc. **609**, A1551 (2000).
[7] M. Meaudre, R. Meaudre, R. Butte, S. Vignoli, C. Longeaud, J. P. Kleider, and P. Roca i Cabarrocas, J. Appl. Phys. **86**, 946 (1999).
[8] P. Roca i Cabarrocas, A. Fontcuberta i Morral, and Y. Poissant, Thin Solid Films **403–404**, 39 (2002).
[9] R. Butte, R. Meaudre, M. Meaudre, S. Vignoli, C. Longeaud, J. P. Kleider, and P. Roca i Cabarrocas, Philos. Mag. B **79**, 1079 (1999).
[10] C. Longeaud, J. P. Kleider, P. Roca i Cabarrocas, S. Hamma, R. Meaudre, and M. Meaudre, J. Non-Cryst. Solids **227–230**, 96 (1998).
[11] R. Butte, S. Vignoli, M. Meaudre, R. Meaudre, O. Marty, L. Saviot, and P. Roca i Cabarrocas, J. Non-Cryst. Solids **266**, 263 (2000).
[12] A. Fontcuberta i Morral, Ph.D. thesis, Ecole Polytechnique, 2001.
[13] A. Fontcuberta i Morral and P. Roca i Cabarrocas, Thin Solid Films **383**, 161 (2001).
[14] O. Saadane, S. Lebib, A. V. Kharchenko, C. Longeaud, and R. Roca i Cabarrocas, J. Appl. Phys. **93**, 9371 (2003).
[15] S. Sriraman, S. Agarwal, E. S. Aydil, and D. Maroudas, Nature (London) **418**, 62 (2002).
[16] T. J. Belich, S. Thompson, C. R. Perrey, U. Kortshagen, C. B. Carter, and J. Kakalios, Mater. Res. Soc. Symp. Proc. **762**, A14 (2003).
[17] D. B. Williams and C. B. Carter, *Transmission Electron Microscopy* (Plenum, New York, 1996).
[18] Y. Watanabe, M. Shiratani, T. Fukuzawa, and H. Kawasaki, Plasma Sources Sci. Technol. **3**, 355 (1994).
[19] L. Boufendi and A. Bouchoule, Plasma Sources Sci. Technol. **3**, 262 (1994).
[20] L. Bouchoule, A. Plain, L. Boufendi, J. P. Blondeau, and C. Laure, J. Appl. Phys. **70**, 1991 (1991).
[21] L. Boufendi, J. Gaudin, S. Huet, G. Viera, and M. Dudemaine, Appl. Phys. Lett. **79**, 4301 (2001).
[22] A. Bouchoule and L. Boufendi, Plasma Sources Sci. Technol. **2**, 204 (1993).
[23] P. Belenguer, J. P. Bondeau, M. Toogood, A. Plain, A. Bouchoule, C. Laure, and J. P. Bouef, Phys. Rev. A **46**, 7923 (1992).
[24] C. Böhm and J. Perrin, J. Phys. D **24**, 865 (1991).
[25] Z. Shen and U. Kortshagen, J. Vac. Sci. Technol. A **20**, 153 (2001).
[26] A. V. Kharchenko, V. Suendo, and P. Roca i Cabarrocas, Thin Solid Films **427**, 236 (2003).
[27] G. Viera, J. Costa, F. J. Compte, F. J. Garcia, J. L. Andujar, and E. Bertran, Vacuum **53**, 1 (1999).

[28]K. Urban and M. Lentzen, Microsc. Microanal. **8**, 8 (2002).
[29]M. Lentzen, B. Jahnen, C. L. Jia, A. Thurst, K. Tillmann, and K. Urban, Ultramicroscopy **92**, 233 (2002).
[30]M. Lentzen, C. L. Jia, and K. Urban, Microsc. Microanal. **9**, 932 (2003).
[31]C. L. Jia, J. Rodriguez Contreras, J. Schubert, M. Lentzen, U. Poppe, H. Kohlstedt, K. Urban, and R. Waser, J. Cryst. Growth **247**, 381 (2003).
[32]C. L. Jia, M. Lentzen, and K. Urban, Science **299**, 870 (2003).
[33]M. Haider, H. Rose, S. Uhlemann, E. Schwan, B. Kabius, and K. Urban, Ultramicroscopy **75**, 53 (1998).
[34]M. Haider, S. Uhlemann, E. Schwann, H. Rose, B. Kabius, and K. Urban, Nature (London) **392**, 768 (1998).
[35]M. Vanecek, J. Kocka, A. Poruba, and A. Fejfar, J. Appl. Phys. **78**, 6203 (1995).
[36]P. Sladek, P. St'ahel, P. Roca i Cabarrocas, and P. Morin, Philos. Mag. B **77**, 1049 (1998).
[37]J. Kocka, M. Vanececk, and A. Triska, in *Amorphous Silicon and Related Materials*, edited by H. Fritzsche (World Scientific, Teanech, NJ, 1988), Vol. 1.
[38]S. Knief and W. von Niessen, Phys. Rev. B **59**, 12940 (1999).
[39]G. D. Cody, T. Tiedje, B. Abeles, B. Brooks, and Y. Goldstein, Phys. Rev. Lett. **47**, 1480 (1981).
[40]F. Urbach, Phys. Rev. **92**, 1324 (1953).
[41]J. Tauc, R. Grigorivici, and A. Vancu, Phys. Status Solidi **15**, 627 (1966).
[42]S. R. Arekat, J. Non-Cryst. Solids **224**, 201 (1998).
[43]P. Bletzinger and M. J. Flemming, J. Appl. Phys. **62**, 4688 (1987).
[44]*High-Resolution Transmission Electron Microscopy and Associated Techniques*, edited by P. Buseck, J. Cowley, and L. Eyring (Oxford University Press, New York, 1988).
[45]C. R. Perrey, C. B. Carter, and M. Lentzen, Microsc. Microanal. **9**, 958 (2003).
[46]C. R. Perrey, S. Thompson, M. Lentzen, U. Kortshagen, and C. B. Carter, J. Non-Cryst. Solids **343**, 78 (2004).
[47]G. Viera, S. Huet, M. Mikikian, and L. Boufendi, Thin Solid Films **403**, 467 (2002).
[48]G. Viera, M. Mikikian, E. Bertran, P. Roca i Cabarrocas, and L. Boufendi, J. Appl. Phys. **92**, 4684 (2002).
[49]A. Fontcuberta i Morral, R. Brenot, E. A. G. Hamers, R. Vanderhaghen, and P. Roca i Cabarrocas, J. Non-Cryst. Solids **266–269**, 48 (2000).
[50]H. Curtins and M. Favre, in *Amorphous Silicon and Related Materials*, edited by H. Fritzsche (World Scientific, Teaneck, NJ, 1988), Vol. 1.
[51]G. D. Cody, in *Semiconductors and Semimetals*, edited by J. I. Pankove (Academic, New York, 1984), p. 11.
[52]N. M. Amer and W. B. Jackson, in *Semiconductors and Semimetals*, edited by J. I. Pankove (Academic, New York, 1984), Vol. 21B, p. 83.
[53]A. R. Middya, S. Hazra, S. Ray, A. K. Barua, and C. Longeaud, J. Non-Cryst. Solids **200**, 1067 (1996).